Graph Neural Networks for Morphometric Characterization of the Aortic Valve

Kamil Ibragimov[1](✉), Matija Jelenc[2], and Tomaž Vrtovec[1]

[1] University of Ljubljana, Faculty of Electrical Engineering, Ljubljana, Slovenia
[2] University Medical Center Ljubljana, Ljubljana, Slovenia
kamil.ibragimov@fe.uni-lj.si

Abstract. Clinically significant geometrical measurements of the aortic valve, such as the intercommissural distances and angles, are enabled by aortic valve morphometry. While morphometry typically relies on detecting key anatomical landmarks of the aortic valve (nadirs and commissures), the accuracy of morphometric measurements derived from these landmarks remains under-investigated. In this study, we devise a graph-based representation, where morphometric measurements of the aortic valve are represented as graph nodes, and their anatomical relationships are represented as graph edges that encode the dependencies of the underlying landmarks. Such representations, which therefore encapsulate the geometric variability of landmark detection, are optimized through a graph neural network (GNN) that integrates geometric features and structural context to compute anatomically consistent morphometric measurements. The proposed GNN approach was evaluated on 280 cardiac computed tomography images consisting of three cohorts from two different institutions with both healthy and pathological aortic valve cases. By computing 29 different morphometric measurements (18 linear and 11 angular) with the proposed GNN approach and comparing them to those obtained from direct landmark detection, we observed a reduction in the mean absolute error by around 15−25% on average. The results demonstrate an improved anatomical consistency of the proposed GNN approach in extracting morphometric measurements, and its robustness to landmark detection uncertainty.

Keywords: Cardiac computed tomography · Aortic valve · Landmark detection · Morphometry · Graph neural network

1 Introduction

Cardiovascular diseases are the leading cause of morbidity and mortality worldwide, placing a significant burden on healthcare systems [14]. Accurate anatomical characterization of the heart and major vessels is the first step in diagnosis, treatment planning and risk stratification for structural heart diseases, especially those affecting the aortic valve [16]. Clinically significant geometrical measurements of the aortic valve, such as the intercommissural distances and angles or basal ring dimensions, are enabled by aortic valve morphometry, and forms the

basis for planning of several surgical procedures, such as the transcatheter aortic valve replacement (TAVR) or aortic valve repair [3,11]. A fundamental element of aortic valve morphometry is the localization of its key anatomical landmarks, which is in medical images commonly performed manually, meaning that it is time-consuming and prone to observer variability. To automate this task, deep learning (DL) methods have emerged and are increasingly being used, demonstrating promising landmark localization accuracy and reproducibility.

Related Work. The aortic root and aortic valve are complex anatomical systems, and their accurate three-dimensional (3D) quantitative assessment is of fundamental importance for planning cardiac surgical procedures [21]. Modern cardiac computed tomography (CT) provides high-resolution images that allow us to understand and reconstruct the spatial geometry of the valve structures. While early work was based primarily on traditional image processing and geometric modeling methods [10,4], DL methods have been actively used in recent years, and can be broadly categorized into three groups. The *first group* focuses on the automatic segmentation of anatomical structures, including the aortic root and valve leaflets. Common architectures are based on convolutional neural networks (CNN), such as U-Net [2] and nnU-Net [8], which demonstrate high accuracy in the selection of anatomical regions and are often used as a preprocessing step for subsequent analysis. In a number of studies, segmentation is supplemented with postprocessing and clustering algorithms to refine boundaries and analyze the structures [23,15,26,13]. The *second group* is devoted to the automatic detection of key anatomical landmarks of the aortic valve, where both CNN architectures with coordinate regression and heatmap-based methods such as spatial configuration networks are commonly used [20], and often implemented as two-stage schemes with coarse and fine landmark localization [12,1,17]. Modern solutions take into account spatial relationships between landmarks through the training of configuration constraints [22,25,27]. However, optimization in these works is mainly aimed at minimizing landmark localization errors, while the derived morphometric measurements remain secondary. The *third group* focuses on the construction of 3D models of the aortic valve and the calculation of morphometric characteristics based on them. Such works use segmentation CNNs to reconstruct the geometry of the leaflets and aortic root, followed by the calculation of volumetric and linear parameters [19].

Motivation. Existing methods for aortic valve morphometry optimize landmark coordinates rather than morphometric measurements, however, relying solely on landmark detection may not be sufficient for a reliable aortic valve morphometry, as errors in landmark detection can propagate to the derived measurements [5]. Morphometric measurements are not independent but are constrained by geometric and physiological relationships that may not be captured by landmark detection and are not explicitly modeled. To address this issue, we focus on improving the measurement accuracy rather than improving landmark detection, and propose a framework based on the graph neural network

(GNN) [9,24] in which morphometric measurements are represented as graph nodes connected with edges according to their common anatomical landmarks. The measurements obtained from landmark detection serve as node inputs, and GNN learns to refine them using the relationships among measurements, allowing for more anatomically consistent and accurate morphometric assessment compared to those obtained from raw landmark detection results.

Contributions. The main contributions of this study are: (1) Formulation of the morphometric analysis of the aortic valve as a graph problem, where individual morphometric measurements are represented as graph nodes and their anatomical relationships are encoded as edges. (2) Development of a GNN model that captures geometric and anatomical dependencies between measurements and provides anatomically consistent refinement of values derived from landmark detection. (3) Integration of inter-parametric constraints into the assessment of complete aortic valve morphometry, enabling joint optimization of related measurements rather than independent post-processing. (4) Experimental validation demonstrating improved accuracy and reproducibility of morphometric measurements without modifying the landmark detection stage.

2 Methods

Morphometric analysis of the aortic valve is based on identifying its key anatomical landmarks, i.e. the nadirs of the right-coronary, left-coronary and non-coronary sinus (i.e. R, L and N, respectively), and the right-/left-coronary, right-/non-coronary and left-/non-coronary commissures (i.e. RLC, RNC and LNC, respectively). From subsets of these landmarks, linear (i.e. basal ring and sino-tubular junction geometry, inter-commissural distances, commissural and centroid valve heights, commissural diameter) or angular (i.e. planar, vertical and commissural triangle angles) morphometric measurements (Table 1) [7] are computed using deterministic geometric operations including Euclidean distances, angles between vectors or plane normals, centroid-based angular calculations, and ellipse fitting.

Landmarks and Landmark Candidate Points. Let the key anatomical landmarks form a set $\mathcal{L} = \{l_i : (x_i, y_i, z_i);\ i = 1, \ldots, N\}$ of size N as the number of landmarks. We treat 3D landmark detection as a segmentation task [8], where each landmark is modeled by a spherical binary mask of radius r. Instead of direct coordinate regression, we therefore construct a probability map for each landmark $l_i \in \mathcal{L}$, which proved to be more stable due to anatomical variability and noise in CT data [18]. From the obtained probability map, N_i candidates for landmark l_i are extracted, first by calculating the center of mass (CoM) p_{i1} of the probability map, which corresponds to the most probable location and represents the main candidate point, and then by selecting additional $N_i - 1$ high-probability points p_{ik} that are at least for distance d apart from the already

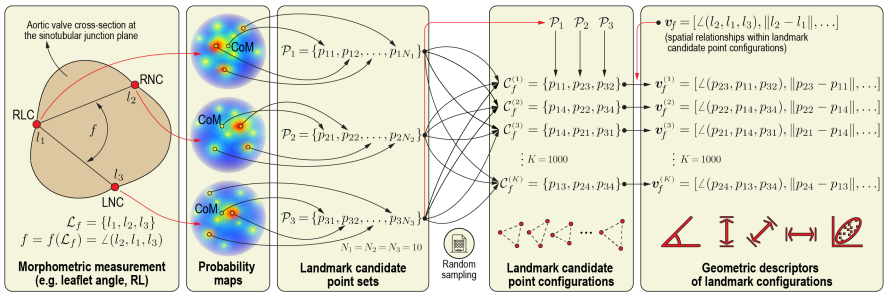

Fig. 1. An illustration of the proposed graph-based representation of landmark detection as the basis for the GNN approach to morphometric analysis of the aortic valve.

selected candidates. If several points have similar probability values, priority is given to those that are closer to CoM. For each landmark $l_i \in \mathcal{L}$, we therefore generate a set of N_i candidate points $\mathcal{P}_i = \{p_{i1}, \ldots, p_{iN_i}\}$ that are concentrated in the corresponding area of high confidence (Fig. 1), allowing us to explicitly take into account the detection uncertainty for subsequent morphometric analysis.

Graph-Based Representation. For a given morphometric measurement f, we define the subset of landmarks $\mathcal{L}_f \subseteq \mathcal{L}$ that are required to compute f, i.e. $f = f(\mathcal{L}_f)$. Let $\mathcal{L}_{f_m}$ and $\mathcal{L}_{f_n}$ be the landmark subsets required for two morphometric measurements f_m and f_n, respectively, where both measurements may share common landmarks, i.e. $\mathcal{L}_{f_m} \cap \mathcal{L}_{f_n} \subseteq \mathcal{L}_{f_m}, \mathcal{L}_{f_n}$. This interdependence motivates us to represent the set of all M morphometric measurements as an undirected graph [6], where each node corresponds to one measurement, and edges form connections between measurements. The connection strength is quantified as the normalized set overlap $q_{mn} = |\mathcal{L}_{f_m} \cap \mathcal{L}_{f_n}| \,/\, |\mathcal{L}_{f_m} \cup \mathcal{L}_{f_n}|$, which ensures that measurements depending on exactly the same landmarks are assigned the maximal strength (i.e. self-loops; $q = 1$), while disjoint measurements are assigned the minimal strength (i.e. no connection; $q = 0$). The outcome of this procedure is a symmetric adjacency matrix $\boldsymbol{Q} = [q_{mn}] \in \mathbb{R}^{M \times M}$, where each element captures how strongly f_m and f_n are linked. Such a graph-based representation provides a natural structure for the morphometric data, as it encodes the dependencies imposed by the anatomy and ensures that each measurement is not treated as an isolated quantity but as part of a connected system defined by the underlying landmarks.

Once the graph has been defined, each node corresponding to a morphometric measurement f must be endowed with numerical information that reflects both the raw candidate values and their associated uncertainty. For each subset of landmarks $\mathcal{L}_f$ required to compute f, we first extract the corresponding collection of candidate point sets $\{\mathcal{P}_{i|f} : l_i \in \mathcal{L}_f\}$. By randomly sampling one candidate point from each set $\mathcal{P}_{i|f}$, we obtain a configuration $\mathcal{C}_f = \{p_{l_i} : l_i \in \mathcal{L}_f\}$ of candidate points for f. We then compute a geometric descriptor vector $\boldsymbol{v}_f(\mathcal{C}_f) = [v_{f1}, \ldots, v_{fV}]$, with its first element $v_{f1} = f(\mathcal{C}_f)$ representing the morphometric measurement

for the current configuration, and additional $V-1$ elements representing the geometric descriptors that capture the spatial relationships within $\mathcal{C}_f$. Their definition depends on the number of landmarks in $\mathcal{L}_f$; if two or more landmarks are present, we compute pairwise Euclidean distances and their mean; if three or more landmarks are present, we compute orientation features (i.e. angle cosine similarities); for larger sets of landmarks we compute descriptors of anisotropy (i.e. eigenvalues of the covariance matrix of the candidate coordinates). Finally, the compactness relative to the centroid of $\mathcal{C}_f$ is included as a measure of how tightly the sampled points cluster, as it describes the spatial dispersion and overall scale of landmark configuration, therefore complementing pairwise distances with a rotation-invariant global descriptor. Finally, we generate a collection of K candidate geometric descriptors $\mathcal{V}_f = \{\boldsymbol{v}_f^{(1)}, \boldsymbol{v}_f^{(2)}, \ldots, \boldsymbol{v}_f^{(K)}\}$ (Fig. 1) that are assigned to node f. The graph nodes therefore do not carry single deterministic values but rather collections of candidate geometric descriptors, derived from sampled landmark combinations and representing the geometric variability of the underlying landmark detection.

Graph Neural Network. To derive the optimal morphometric measurements from the devised graph representation, we devised a GNN [9,24]. For each measurement f, the candidate geometric descriptors $\mathcal{V}_f$ are mapped row-wise into an embedding space of fixed dimension E using a multi-layer perceptron (MLP) by preserving the candidate axis, i.e. the output for each f is matrix $\boldsymbol{H}_f^0 \in \mathbb{R}^{K\times E}$, so every candidate retains its own representation. To share information among interdependent measurements, we use graph convolutional layers. At each layer ℓ, the candidate embeddings of node f are mean-pooled into a context vector $\boldsymbol{c}_f^{(\ell)} \in \mathbb{R}^E$, and collecting these vectors across all M measurements forms a matrix of node contexts $\boldsymbol{C}^{(\ell)} = [\boldsymbol{c}_f^{(\ell)}] \in \mathbb{R}^{M\times E}$. A graph convolution then updates these contexts according to $\boldsymbol{C}^{(\ell+1)} = \sigma(\boldsymbol{D}^{-1/2}\,\boldsymbol{Q}\,\boldsymbol{D}^{-1/2}\,\boldsymbol{C}^{(\ell)}\,\boldsymbol{W}^{(\ell)})$, where $\boldsymbol{D} = [d_{mm} = \sum_n q_{mn}]$ is the diagonal degree matrix of the adjacency matrix $\boldsymbol{Q} = [q_{mn}]$, $\boldsymbol{W}$ is a learnable weight matrix and $\sigma(\cdot)$ is the ReLU activation function. The aim of $\boldsymbol{C}$ is to continuously update the context of each measurement node by considering its neighbors, and the updated node context $\boldsymbol{c}_f^{(\ell)}$ is then injected back into the corresponding candidate representations for measurement f. This is achieved by broadcasting $\boldsymbol{c}_f^{(\ell)}$ to match the number of candidates K, concatenating it with each candidate embedding from the previous layer, and applying a small residual MLP to obtain $\boldsymbol{H}_f^{(\ell+1)} = \boldsymbol{H}_f^{(\ell)} + \mathrm{MLP}\big([\boldsymbol{H}_f^{(\ell)}, \mathbf{1}_K \boldsymbol{c}_f^{(\ell)}]\big)$, where $\mathbf{1}_K$ is the unit column vector of length K. This fusion ensures that candidate embeddings evolve across layers, influenced both by their own features and by the anatomical context provided through the graph. After L layers, each node still holds a candidate matrix $\boldsymbol{H}_f^{(L)} \in \mathbb{R}^{K\times E}$, which passes through an MLP to obtain a scalar score for each candidate, and for all candidates, the softmax function produces weights $\mathcal{A} = \{\alpha_{f1}, \ldots, \alpha_{fK}\}$. Considering the first element of each geometric descriptor $\boldsymbol{v}_f^{(k)}$ represents the morphometric measurement, (i.e. $v_{f1} = f(\mathcal{C}_f)$), its final prediction f_{GNN} is the weighted sum of candidate values, computed as $f_{\mathrm{GNN}} = \sum_{k=1}^{K} \alpha_{fk}\, v_{f1}^{(k)}$. Essentially, GNN does not regress the values

for the measurements directly but selects among anatomically plausible candidates, guided by both geometric descriptors and graph-based context. The GNN model is trained end-to-end using a mean squared error loss computed jointly across all predicted measurements without any auxiliary losses, measurement-specific weighting or additional regularization terms.

3 Experiments and Results

Dataset. We collected three cohorts of cardiac CT images from two institutions in accordance with clinical protocols for aortic root and valve assessment: 151 healthy subjects and 61 subjects with dilation of the aortic root and/or ascending aorta from institution 1, and additional 68 subjects with the same pathology from institution 2. Images were acquired with matrix size of 512×512, number of slices $228-1327$, and pixel size of $(0.35-0.84) \times (0.35-0.84) \times (0.3-1.5)$ mm. From each cohort, 15 subjects were randomly selected for testing, and the remaining were used for training. For all subjects, ground-truth annotations of $N = 6$ key anatomical landmarks of the aortic valve (i.e. $\mathcal{L} = \{\mathrm{R}, \mathrm{L}, \mathrm{N}, \mathrm{RLC}, \mathrm{RNC}, \mathrm{LNC}\}$) were performed manually by an experienced cardiovascular surgeon.

Experiments. Our morphometric analysis of the aortic valve starts with landmark detection, treated as a nnU-Net [8] segmentation task with default configuration and automatic hyperparameter selection, for which the spherical binary masks were constructed with a radius of $r = 3.6$ mm that was experimentally determined on the $[1.6, 4.4]$ mm interval. Each i-th landmark was represented by $N_i = 10$ candidate points $\mathcal{P}_i$, i.e. the CoM of the resulting probability map, and additional high-probability locations at least $d = 1.0$ mm apart. The candidate points were then fed to our graph-based representation, which by random sampling produced $K = 1000$ candidate geometric descriptors $\boldsymbol{v}_f$ for each observed morphometric measurement f, and through GNN optimization [9] resulted in the predicted f_{GNN}. To verify whether the proposed GNN approach improves the measurement accuracy, we computed each morphometric measurement directly from the detected landmarks as f_{CoM}, i.e. by using CoM of each nnU-Net probability map for the corresponding landmark location. Both f_{CoM} and f_{GNN} were compared to reference morphometric measurements f_{GT}, obtained from ground-truth landmark annotations.

Implementation Details. GNN consisted of $L = 2$ graph convolutional layers implemented in PyTorch, each followed by context injection into candidate embeddings. Model training was performed using the Adam optimizer with a learning rate of 10^{-5} and the maximum number of epochs set to 10,000, with input geometric descriptors normalized prior to training to ensure numerical stability. All training and evaluation procedures were conducted on three 12 GB NVIDIA GeForce RTX 2080 Ti graphics processing units.

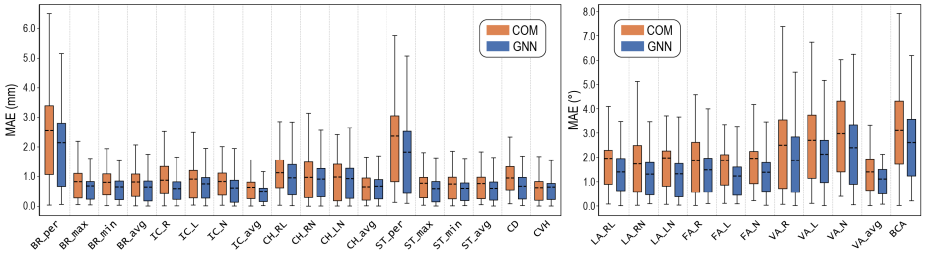

Fig. 2. Mean absolute error (MAE) boxplots of linear (*left*) and angular (*right*) morphometric measurements of the aortic valve (Table 1) for the direct center of mass (CoM) and our proposed graph neural network (GNN) approach.

Results. Landmark detection using the nnU-Net segmentation heatmaps resulted in a localization error of up to 0.95 mm for 99.4% of landmarks (for only two landmarks, it exceeded $r = 3.6$ mm). We then evaluated the mean absolute error (MAE) of CoM and GNN morphometric measurements against reference measurements (18 linear and 11 angular; $M = 29$ in total), with the results reported in Table 1 and Fig. 2. In most cases, the proposed GNN approach demonstrated a lower MAE in comparison to CoM, with an average gain of $\sim$15$-$25%.

Observer variability. In terms of normalized MAE, the proposed GNN approach achieved an error of $2.5 \pm 0.9\%$ for linear and $9.6 \pm 10.2\%$ for angular measurements. For a subset of 25 cases with repeated ground-truth annotations of landmarks $\mathcal{L}$, the inter-observer variability was respectively $3.0 \pm 1.6\%$ and $15.4 \pm 15.8\%$, while the intra-observer variability was respectively $1.6 \pm 1.0\%$ and $8.4 \pm 9.5\%$, indicating that the proposed framework performs within the range of inter-observer and close to the limits of intra-observer variability.

4 Discussion

We proposed an approach for the morphometric analysis of the aortic valve that shifts the focus from standard key landmark detection [1,17] to the refinement of the derived morphometric measurements by adopting a GNN approach.

Morphometric Measurement Accuracy. Our results demonstrate that even with a fixed landmark detection stage, explicitly modeling anatomical relationships between parameters considerably reduces errors in clinically relevant geometric features. This highlights that minimizing coordinate errors alone does not guarantee optimal morphometric measurement accuracy, particularly when measurements depend on multiple anatomical landmarks. By representing morphometric measurements as graph nodes and encoding their dependencies via graph edges, the method enforces anatomical consistency across distances and

Table 1. Mean absolute error (MAE) in terms of mean ± standard deviation of linear and angular morphometric measurements of the aortic valve (based on the reported set of landmarks) for the direct center of mass (CoM) and our proposed graph neural network (GNN) approach (best results are in bold).

Morphometric measurement: `label`	Landmarks	CoM	GNN
Linear measurements		MAE (mm) ↓	
Basal ring perimeter: `BR_per`	R|L|N	2.54 ± 2.03	$\mathbf{2.14 \pm 1.94}$
Basal ring diameter, max: `BR_max`		0.82 ± 0.66	$\mathbf{0.67 \pm 0.63}$
Basal ring diameter, min: `BR_min`		0.80 ± 0.64	$\mathbf{0.64 \pm 0.61}$
Basal ring diameter, mean: `BR_avg`		0.81 ± 0.64	$\mathbf{0.64 \pm 0.61}$
Intercommissural distance, R: `IC_R`	RLC|RNC	0.87 ± 0.55	$\mathbf{0.58 \pm 0.47}$
Intercommissural distance, L: `IC_L`	RLC|LNC	0.90 ± 0.82	$\mathbf{0.75 \pm 0.71}$
Intercommissural distance, N: `IC_N`	LNC|RNC	0.83 ± 0.60	$\mathbf{0.61 \pm 0.52}$
Intercommissural distance, mean: `IC_avg`	RLC|RNC|LNC	0.63 ± 0.58	$\mathbf{0.50 \pm 0.40}$
Commissural height, RL: `CH_RL`	All	1.12 ± 0.82	$\mathbf{0.95 \pm 0.79}$
Commissural height, RN: `CH_RN`		0.96 ± 0.84	$\mathbf{0.91 \pm 0.71}$
Commissural height, LN: `CH_LN`		0.97 ± 1.00	$\mathbf{0.92 \pm 0.98}$
Commissural height, mean: `CH_avg`		$\mathbf{0.65 \pm 0.64}$	0.66 ± 0.66
Sinotubular junction perimeter: `ST_per`	RLC|RNC|LNC	2.37 ± 2.02	$\mathbf{1.82 \pm 1.77}$
Sinotubular junction diam., max: `ST_max`		0.77 ± 0.63	$\mathbf{0.58 \pm 0.56}$
Sinotubular junction diam., min: `ST_min`		0.74 ± 0.66	$\mathbf{0.59 \pm 0.57}$
Sinotubular junction diam., mean: `ST_avg`		0.75 ± 0.64	$\mathbf{0.60 \pm 0.56}$
Commissural diameter: `CD`	RLC|RNC|LNC	0.94 ± 0.56	$\mathbf{0.66 \pm 0.51}$
Centroid valve height: `CVH`	All	$\mathbf{0.62 \pm 0.64}$	0.64 ± 0.66
Angular measurements		MAE (°) ↓	
Leaflet angle, RL: `LA_RL`	RLC|RNC|LNC	1.96 ± 1.49	$\mathbf{1.40 \pm 1.09}$
Leaflet angle, RN: `LA_RN`		1.73 ± 1.39	$\mathbf{1.31 \pm 1.03}$
Leaflet angle, LN: `LA_LN`		1.97 ± 1.79	$\mathbf{1.32 \pm 1.17}$
Flat angle, R: `FA_R`	RLC|RNC|LNC	1.86 ± 1.52	$\mathbf{1.48 \pm 1.17}$
Flat angle, L: `FA_L`		1.87 ± 1.71	$\mathbf{1.23 \pm 1.10}$
Flat angle, N: `FA_N`		1.96 ± 1.56	$\mathbf{1.39 \pm 1.12}$
Vertical angle, R: `VA_R`	All	2.50 ± 2.08	$\mathbf{1.87 \pm 1.96}$
Vertical angle, L: `VA_L`		2.70 ± 2.15	$\mathbf{2.12 \pm 1.64}$
Vertical angle, N: `VA_N`		2.97 ± 2.32	$\mathbf{2.39 \pm 2.10}$
Vertical angle, mean: `VA_avg`		1.40 ± 1.07	$\mathbf{1.10 \pm 0.90}$
Basal/commissural plane angle: `BCA`	All	3.10 ± 1.96	$\mathbf{2.60 \pm 1.67}$

angles. Unlike traditional post-processing approaches, the graph explicitly integrates structural constraints, allowing GNN to optimize competing candidate configurations. The evaluation included both healthy subjects and cases with aortic valve pathology, and the results indicate that the proposed GNN approach is robust to landmark detection uncertainty.

Limitations. The main limitation of the proposed approach is that GNN is not a standalone landmark detector, but a refinement module requiring initial landmark proposals. As a result, errors from the landmark detection stage may still propagate to the morphometric measurement stage. Although we tackled this problem by introducing probability maps that result from treating landmark detection as a segmentation problem, poor initial detection may still cause the GNN-based refinement to fail.

5 Conclusions

This paper introduced a GNN-based approach to automated morphometric analysis of the aortic valve, in which the task of improving the accuracy of morphometric measurements is formulated as a graph problem. The devised graph-based representation takes into account the anatomical relationships between morphometric measurements, and refines the derived measurements through GNN without changing the stage of their detection. The results demonstrate that taking into account the inter-measurement dependencies improves the morphometric measurement accuracy.

Data and Code Availability. The data used in this study are available from the corresponding author upon reasonable request. The code is publicly available at https://github.com/kam-ibragimov/morpho-gcn.

Acknowledgments. This study was approved by the National Medical Ethics Committee of the Republic of Slovenia under 0120-25/2024-2711-6, and was funded by the Slovenian Research and Innovation Agency (ARIS) under J2-50067 and P2-0232.

Disclosure of Interests. The authors have no competing interests to declare.

References

1. Aoyama, G., Zhao, L., Zhaoand, S., et al.: Automatic aortic valve cusps segmentation from CT images based on the cascading multiple deep neural networks. J Imaging **8**, 11 (2022). https://doi.org/10.3390/jimaging8010011
2. Çiçek, O., Abdulkadir, A., Lienkamp, S.S., Brox, T., Ronneberger, O.: 3D U-Net: Learning dense volumetric segmentation from sparse annotation. In: 19th International Conference on Medical Image Computing and Computer-Assisted Intervention – MICCAI 2016, Lect Notes Comput Sci, vol. 9901, pp. 424–432. Springer (2016). https://doi.org/10.1007/978-3-319-46723-8_49
3. Dudkiewicz, D., Lis, M., Yakovliev, A., et al.: Aortic root morphometry revisited-Clinical implications for aortic valve interventions. Clin Anat **37**, 719–729 (2024). https://doi.org/10.1002/ca.24165
4. Elattar, M., Wiegerinck, E., van Kesteren, F., et al.: Automatic aortic root landmark detection in CTA images for preprocedural planning of transcatheter aortic valve implantation. Int J Cardiovasc Imaging **32**, 501–511 (2015). https://doi.org/10.1007/s10554-015-0793-9

5. Engelkes, K., Helfsgott, J., Hammel, J.U., et al.: Measurement error in μct-based three-dimensional geometric morphometrics introduced by surface generation and landmark data acquisition. Journal of Anatomy **235**(2), 357–378 (2019). https://doi.org/10.1111/joa.12999
6. Grinberg, D.: An introduction to graph theory. arXiv:2308.04512 (2025). https://doi.org/10.48550/arXiv.2308.04512
7. Ho, S.Y.: Structure and anatomy of the aortic root. Eur J Echocardiogr **10**, i3–i10 (2009). https://doi.org/10.1093/ejechocard/jen243
8. Isensee, F., Jaeger, P.F., Kohl, S.A.A., Petersen, J., Maier-Hein, K.H.: nnU-Net: Self-adapting framework for U-Net-based medical image segmentation. Nat Methods **18**, 203–211 (2021). https://doi.org/10.1038/s41592-020-01008-z
9. Kipf, T.N., Welling, M.: Semi-supervised classification with graph convolutional networks. arXiv:1609.02907 (2017). https://doi.org/10.48550/arXiv.1609.02907
10. Lalys, F., Esneault, S., Castro, M., et al.: Automatic aortic root segmentation and anatomical landmarks detection for TAVI procedure planning. Minim Invasive Ther Allied Technol **28**, 157–164 (2019). https://doi.org/10.1080/13645706.2018.1488734
11. Litmanovich, D.E., Ghersin, E., Burke, D.A., Popma, J., Shahrzad, M., Bankier, A.A.: Imaging in Transcatheter Aortic Valve Replacement (TAVR): role of the radiologist. Insights Imaging **5**, 123–145 (2014). https://doi.org/10.1007/s13244-013-0301-5
12. Ma, Q., Lemarchand, L., Chan-Sock-Line, D., Rigal, L., Simon, A., Haigron, P.: Fully-automatic aortic valve landmarks detection with two-stage-based convolutional neural networks. In: SPIE Medical Imaging 2023: Image Processing. vol. 12464, p. 124643K (2023). https://doi.org/10.1117/12.2645635
13. Mao, Y., Zhu, G., Yang, T., et al.: Rapid segmentation of computed tomography angiography images of the aortic valve: the efficacy and clinical value of a deep learning algorithm. Front Bioeng Biotechnol **12**, 1285166 (2024). https://doi.org/10.3389/fbioe.2024.1285166
14. Mensah, G.A., Fuster, V., Murray, C.J.L., Roth, G.A.: Global burden of cardiovascular diseases and risks, 1990–2022: 2022 report of the GBD study. J Am Coll Cardiol **82**, 2350–2473 (2023). https://doi.org/10.1016/j.jacc.2023.11.007
15. Minghini, G., Cavallo, A.U., Miola, A., et al.: An HPC pipeline for calcium quantification of aortic root from contrast-enhanced CCT scans. IEEE Access **11**, 101309–101319 (2023). https://doi.org/10.1109/ACCESS.2023.3315734
16. Mitsis, A., Kyriakou, M., Fouseki, A., et al.: Cardiac computed tomography in structural heart interventions: From preprocedural planning to procedural strategy. Rev Cardiovasc Med **26**, 46998 (2025). https://doi.org/10.31083/RCM46998
17. Noothout, J.M.H., de Vos, B.D., Wolterink, J.M., et al.: Deep learning-based regression and classification for automatic landmark localization in medical images. IEEE Trans Med Imaging **39**, 4011–4022 (2020). https://doi.org/10.1109/TMI.2020.3009002
18. O'Neil, A.Q., Kascenas, A., Henry, J., et al.: Attaining human-level performance with atlas location autocontext for anatomical landmark detection in 3D CT data. In: Computer Vision – ECCV 2018 Workshops, LNCS, vol. 11131, pp. 470–484. Springer (2018). https://doi.org/10.1007/978-3-030-11015-4_34
19. Pak, D.H., Liu, M., Kim, T., et al.: Patient-specific heart geometry modeling for solid biomechanics using deep learning. IEEE Trans Med Imaging **43**, 203–215 (2024). https://doi.org/10.1109/TMI.2023.3294128

20. Payer, C., Štern, D., Bischof, H., Urschler, M.: Integrating spatial configuration into heatmap regression based CNNs for landmark localization. Med Image Anal **54**, 207–219 (2019). https://doi.org/10.1016/j.media.2019.03.007
21. Tretter, J.T., Izawa, Y., Spicer, D.E., et al.: Understanding the aortic root using computed tomographic assessment: a potential pathway to improved customized surgical repair. Circ Cardiovasc Imaging **14**, e013134 (2021). https://doi.org/10.1161/CIRCIMAGING.121.013134
22. Škrlj, L., Jelenc, M., Vrtovec, T.: Detection of aortic cusp landmarks in computed tomography images with deep learning. In: 12th International Conference on Functional Imaging and Modeling of the Heart – FIMH 2023, Lect Notes Comput Sci, vol. 13958, pp. 301–309. Springer (2023). https://doi.org/10.1007/978-3-031-35302-4_31
23. Wang, M., Niu, G., Chen, Y., et al.: Development and validation of a deep learning-based fully automated algorithm for pre-TAVR CT assessment of the aortic valvular complex and detection of anatomical risk factors: a retrospective, multicentre study. eBioMedicine **96**, 104794 (2023). https://doi.org/10.1016/j.ebiom.2023.104794
24. Wu, Z., Pan, S., Chen, F., Long, G., Zhang, C., Yu, P.S.: A comprehensive survey on graph neural networks. IEEE Trans Neural Netw Learn Syst **32**, 4–24 (2021). https://doi.org/10.1109/TNNLS.2020.2978386
25. Yamauchi, H., Aoyama, G., Tsukihara, H., et al.: Deep learning-based fully automated aortic valve leaflets and root measurement from ct images: A feasibility study. Circulation Journal **89**(9), 1499–1509 (2025). https://doi.org/10.1253/circj.CJ-24-1031
26. Zhang, D.Y., Rodighiero, J., Arif, S.G., et al.: Automated quantification of cardiovascular calcifications using deep learning: prognostic value in older adults undergoing TAVR. Preprints Lancet (2023). https://doi.org/10.2139/ssrn.4574756
27. Zou, H., Jiang, Y., Huang, H., et al.: Automated and quantitative assessment of aortic root based on ct angiography using a new deep-learning tool: A comparison study. Quantitative Imaging in Medicine and Surgery **14**(12), 8414–8428 (2024). https://doi.org/10.21037/qims-24-650